Proofs to Prof. M.A. Halcrow,

School of Chemistry, University of Leeds,

Woodhouse Lane, Leeds LS2 9JT, U.K.

Four New Spin-Crossover Salts of $[Fe(3\text{-bpp})_2]^{2+}$

(3-bpp = 2,6-*Bis*[1*H*-pyrazol-3-yl]pyridine)

Paul King, James J. Henkelis, Colin A. Kilner,

and Malcolm A. Halcrow*

School of Chemistry, University of Leeds,

Woodhouse Lane, Leeds, LS2 9JT, U.K.

Fax: +44 113 343 6565

Email: M.A.Halcrow@leeds.ac.uk

Invited submission for the Werner Centenary special issue of *Polyhedron*

TOC Entry

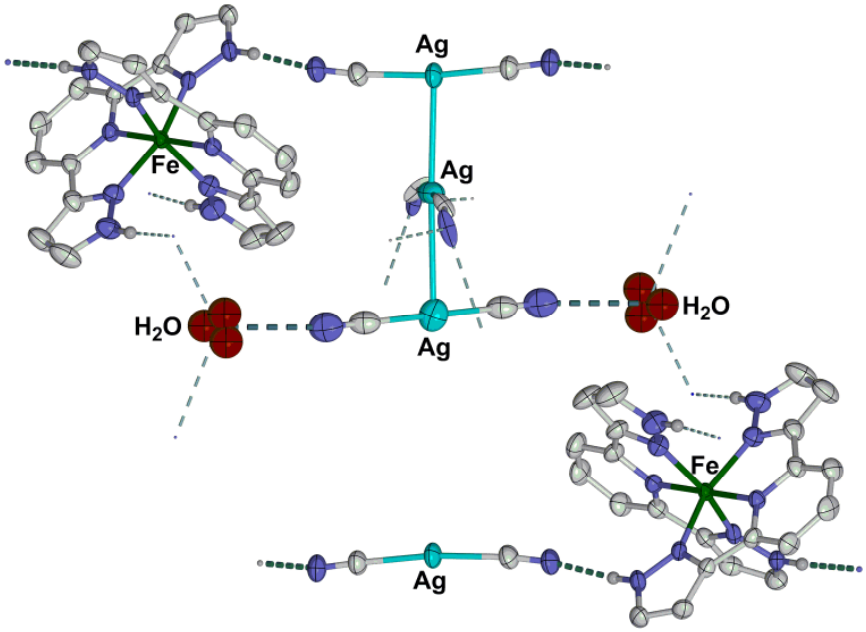

The salts $[Fe(3\text{-}bpp)_2]X_2$ ($X^- = [Ag(CN)_2]^-$, **1**; $X^- = [Au(CN)_2]^-$, **2**; $X^- = [Au(SCN)_2]^-$, **3**; $X^- = BPh_4^-$, **4**) are reported. Compounds **1** and **2** are better formulated as $[Fe(3\text{-}bpp)_2]_2[M(CN)_2][M_3(CN)_6]\cdot 2H_2O$ (M = Ag or Au) on the basis of their crystal structures (as shown). Bulk samples of **1**-**4** all exhibit very gradual thermal spin-state transitions centered at room temperature or below.

Keywords

Iron; Spin-Crossover; Crystal Structure; Magnetic Measurements

ABSTRACT

Four new salts of the well-known spin-crossover centre $[Fe(3\text{-}bpp)_2]^{2+}$ are described: $[Fe(3\text{-}bpp)_2][M(CN)_2]_2$ (M = Ag, **1**; M = Au, **2**), $[Fe(3\text{-}bpp)_2][Au(SCN)_2]_2$ (**3**) and $[Fe(3\text{-}bpp)_2][BPh_4]_2$ (**4**) are reported. Monohydrate crystals of **1** and **2** are isostructural, and are better formulated as $[Fe(3\text{-}bpp)_2]_2[M(CN)_2][M_3(CN)_6]\cdot 2H_2O$ (M = Ag or Au) with the mononuclear and trinuclear anion sites being disordered within each anion dyad. These groups are linked into a 2D network topology through N–H…X (X = N or O) hydrogen bonding between the cations and the cyanometallate anions, and the lattice water. In contrast, the complex cations in the solvate $\mathbf{4}\cdot 2CH_3NO_2\cdot(C_2H_5)_2O$ are completely encapsulated by phenyl groups from the BPh_4^- anions. Dried powder samples of **1**-**4** all exhibit very gradual thermal spin-state transitions centred at $198 \leq T_{½} \leq 291$ K. ES mass spectrometry of **1**-**3** implies that extensive ligand exchange between the iron and coinage metal ions occurs in solution. Solid **1** and **2** are not emissive at room temperature upon irradiation in the UV.

INTRODUCTION

The resurgence in interest in thermally and optically switchable spin-crossover materials [1] in the 1990s was originally driven by the demonstration of their potential for use in display and memory devices [2]. More recently attention has turned to other potential applications for the spin-crossover phenomenon, with several groups preparing multifunctional spin-crossover materials that combine a thermal spin-transition with another physical property [3]. Examples include salts of spin-crossover cations with metal/dithiolene anions, that can combine spin-crossover with electrical conductivity [4]; magnetic metal/oxalate framework structures with included spin-crossover cations [5, 6]; and nanoporous metal-organic frameworks constructed with spin-crossover centres, whose spin-state behaviour is sensitive to the addition or removal of guest solvent [7, 8]. These studies have tended to employ a small selection of spin-crossover cation centres, that are robust in solution and can be crystallised in the presence of potentially coordinating anions. One of these is $[Fe(3\text{-bpp})_2]^{2+}$ (3-bpp = 2,6-*bis*[1*H*-pyrazol-3-yl]pyridine), whose salts have been shown to undergo a variety of thermal spin-state transitions that often show a strong solvent dependence [6, 9-11]. Unusually for a complex of this type, $[Fe(3\text{-bpp})_2]^{2+}$ is stable in aqueous solution at room temperature [11], which facilities the preparation of new salts of this cation by anion metathesis.

We report here four new salts of $[Fe(3\text{-bpp})_2]^{2+}$, with cyanometallate, thiocyanometallate or BPh_4^- anions. The cyanometallate and thiocyanometallate salts were prepared with a view to examining their fluorescence. There is some indication in the literature that the high-and low-spin states of a compound might have different emissive properties [12], and some groups (including ourselves) have succeeded in combining spin-crossover and fluorescence in the same material, albeit not always at the same temperatures [13]. By analogy with the conducting double salts mentioned in the previous paragraph [4], we reasoned that combining

a spin-crossover cation with a fluorescent cyanometallate anion [14, 15] might be a way of achieving that goal. The nucleophilicity of cyanometallate species [16], and the lability of high-spin iron(II) centres, makes the crystallisation of such double salts a challenge. Hence, while network structures constructed from cyanometallate centres are an important class of spin-crossover material [8, 17, 18], the only previously reported discrete salt of a spin-crossover cation with a cyanometallate anion is $[Fe(3\text{-bpp})_2][Fe(CN)_5NO]$ [19]. This undergoes an abrupt thermal spin-transition at 183 K with narrow hysteresis, but its emissive properties were not examined. Therefore, other cyanometallate salts of $[Fe(3\text{-bpp})_2]^{2+}$ were also worthy of investigation. The salt $[Fe(3\text{-bpp})_2][BPh_4]_2$ was synthesised for a different reason, as a reagent for our continuing studies of the supramolecular chemistry of spin-crossover in solution [11].

<Insert Ligand Schematic here>

EXPERIMENTAL

All manipulations were carried out in air, using reagent-grade solvents. 2,6-*Bis*(pyrazol-3-yl)pyridine (3-bpp) [20] and $K[Au(SCN)_2]$ [21] were prepared by previously reported methods, while all other reagents and solvents were used as supplied.

Synthesis of $[Fe(3\text{-bpp})_2][Ag(CN)_2]_2$ (1)

A mixture of $FeCl_2{\cdot}4H_2O$ (0.12 g, 0.59 mmol) and 3-bpp (0.25 g, 1.18 mmol) in water (50 cm^3) was stirred with mild heating until all the solid had dissolved. The resultant orange-brown solution was filtered, and an aqueous solution of $K[Ag(CN)_2]$ (0.23 g, 1.18 mmol in 10 cm^3 H_2O) was slowly added to the filtrate giving an immediate orange precipitate. The precipitate was allowed to settle overnight, then collected by filtration, washed with water and dried *in vacuo*. The solid product is sparingly soluble in most organic solvents, but can

be recrystallised in mg quantities from 2,2,2-trifluoroethanol/diethyl ether to yield plate-like crystals of the monohydrate material. Yield 0.20 g, 64 %. Found C, 39.2; H, 2.20; N, 24.0 %. Calcd. for $C_{26}H_{18}Ag_2FeN_{14}$ C, 39.1; H, 2.27; N, 24.6 %. ES mass spectrum (MeCN) *m*/*z* 212.1 $[3\text{-bpp+H}]^+$, 234.1 $[Na(3\text{-bpp})]^+$, 318.0 $[Ag(3\text{-bpp})]^+$, 445.2 $[Na(3\text{-bpp})_2]^+$, 529.1 $[Ag(3\text{-bpp})_2]^+$, 637.0 $[Fe(3\text{-bpp})_2Ag(CN)_2]^+$. IR (nujol): 3144s, 3096m, 2149, 1615m, 1573m, 1562m, 1540w, 1532m, 1515m, 1435s, 1353m, 1304w, 1281m, 1230w, 1165w, 1148m, 1105w, 1083w, 1068m, 1025w, 996m, 929m, 883m, 841m, 764s, 615m cm^{-1}.

Synthesis of $[Fe(3\text{-bpp})_2][Au(CN)_2]_2$ (2)

Method as for **1**, using $K[Au(CN)_2]$ (0.34 g, 1.18 mol). The product was an orange powder. Yield 0.20 g, 64 %. Found C, 33.0; H, 2.02; N, 19.5 %. Calcd. for $C_{26}H_{18}Au_2FeN_{14}$ C, 32.0; H, 1.86; N, 20.1 %. ES mass spectrum (MeCN) *m*/*z* 212.1 $[3\text{-bpp+H}]^+$, 234.1 $[Na(3\text{-bpp})]^+$, 445.2 $[Na(3\text{-bpp})_2]^+$, 477.1 $[Fe(3\text{-bpp})_2]^+$, 727.1 $[Fe(3\text{-bpp})_2Au(CN)_2]^+$. IR (nujol): 3143s, 3094m, 2147s, 1618m, 1572m, 1561m, 1542w, 1531m, 1513m, 1436s, 1407w, 1352s, 1307w, 1278m, 1232m, 1169w, 1148m, 1105w, 1083w, 1066m, 1028w, 995m, 929m, 883m, 832m, 766s, 692w, 613s cm^{-1}.

Synthesis of $[Fe(3\text{-bpp})_2][Au(SCN)_2]_2 \cdot CF_3CH_2OH$ ($3 \cdot CF_3CH_2OH$)

Method as for **1**, using $K[Au(SCN)_2]$ (0.42 g, 1.18 mol). The product was an orange powder, that formed polycrystalline needles from 2,2,2-trifluoroethanol/diethyl ether. Yield 0.20 g, 64 %. Found C, 27.0; H, 1.90; N, 15.9 %. Calcd. for $C_{26}H_{18}Au_2FeN_{14}S_4$ C, 27.9; H, 1.84; N, 16.3 %. ES mass spectrum (MeCN) *m*/*z* 212.1 $[LH]^+$, 445.2 $[Na(3\text{-bpp})_2]^+$, 477.1 $[Fe(3\text{-bpp})_2]^+$, 523.2 ($[Au(3\text{-bpp–H})(SCN)_2]^+$), 581.1 ($[Fe(3\text{-bpp})Au(SCN)_2]^+$), 735.2 ($[Au(3\text{-bpp})_2(SCN)_2]^+$), 792.2 ($[Fe(3\text{-bpp})_2Au(SCN)_2]^+$). IR (nujol): 3161s, 3134s, 2131s, 1614m, 1573s, 1514m, 1435s, 1353s, 1305m, 1282m, 1233m, 1169m, 1149s, 1104w, 1084m, 1065s, 1019w, 994s, 960w, 927m, 877s, 810s, 767s, 738m, 692w, 667m, 614s cm^{-1}.

Synthesis of $[Fe(3\text{-bpp})_2][BPh_4]_2\cdot xH_2O$ ($4\cdot xH_2O$; $x \approx ½$) A mixture of $FeCl_2\cdot 4H_2O$ (0.12 g, 0.59 mmol) and 3-bpp (0.25 g, 1.18 mmol) in water (50 cm^3) was stirred with mild heating until all the solid had dissolved. The resultant orange-brown solution was filtered, and an aqueous solution of $NaBPh_4$ (0.40 g, 1.18 mmol in 20 cm^3 H_2O) was slowly added to the filtrate giving an immediate yellow precipitate. The solid was collected by filtration, washed with water and dried *in vacuo*. Recrystallisation from $MeNO_2/Et_2O$ yielded yellow plates, which decomposed *in vacuo* to an orange-brown powder. Yield 0.59 g, 89 %. Found C, 74.9; H, 5.15; N, 12.6 %. Calcd. for $C_{70}H_{58}B_2FeN_{10}\cdot ½H_2O$ C, 75.7; H, 5.28; N, 12.4 %. ES mass spectrum (MeCN) *m*/*z* 212.1 $[3\text{-bpp+H}]^+$, 234.1 $[Na(3\text{-bpp})]^+$, 477.1 $[Fe(3\text{-bpp})_2]^+$. IR (nujol) 3584w, 3513w, 3387s, 3346s, 3143m, 3119m, 3054w, 3031w, 1950br w, 1884br w, 1826br w, 1647br w, 1609m, 1579m, 1507w, 1497w, 1531w, 1359s, 1303w, 1274m, 1216m, 1090m, 1065m, 1032m, 991m, 971w, 960w, 931m, 916w, 864w, 845m, 812m, 775s, 744s, 737s, 709s, 670w, 642w, 628w, 610m cm^{-1}.

Single crystal X-ray structure determinations

Orange-brown plates of **1**·H_2O and **2**·H_2O were grown by slow diffusion of diethyl ether vapour into solutions of the compounds in 2,2,2-trifluoroethanol. A similar vapour diffusion into a solution of **4**·xH_2O in nitromethane afforded large yellow needles of **4**·$2CH_3NO_2\cdot(C_2H_5)_2O$. Diffraction data were measured using a Bruker X8 Apex diffractometer fitted with an Oxford Cryostream cooling device, using graphite-monochromated Mo-K_α radiation (λ = 0.71073 Å) generated by a rotating anode. The structures were all solved by direct methods using *SHELXS97* [22], then developed by least squares refinement on F^2 with *SHELXL97* [22]. All crystallographic figures were prepared using *X-SEED* [23], which incorporates *POVRAY* [24]. Experimental details from these structure determinations are summarized in Table 1.

<Insert Table 1 here>

Crystals of **1**·H_2O and **2**·H_2O are isostructural, with asymmetric units containing one complex cation and two $[M(CN)_2]^-$ (M = Ag or Au) anions lying on general lattice sites; and, another $[M(CN)_2]^-$ half-anion lying on the crystallographic inversion centre at the origin. Following initial refinement, one of the two $[M(CN)_2]^-$ moieties occupying a general lattice site [M(42)-N(46)] had substantially higher thermal ellipsoids than the other anion sites in the model. That, and charge-balancing considerations, both implied that this anion site is only half-occupied in the asymmetric unit, and so is disordered about the aforementioned inversion centre. Finally, three Fourier peaks that are not bonded to any other atom, but lie within hydrogen-bonding distance of N(36), were modelled as a disordered water molecule.

In **1**·H_2O, all the non-H atoms except the partial water sites were refined anisotropically, while for **2**·H_2O the wholly occupied non-H atoms plus the half-occupied gold atom Au(42) were refined anisotropically. All C- and N-bound H atoms in both structures were placed in calculated positions and refined using a riding model. The water H atoms could not be located in the Fourier map and so were not included in the final model, but are accounted for in the density and *F*000 calculations. The highest residual Fourier peak for **1**·H_2O of +1.5 $e.Å^{-3}$ is not bonded to any other atom and lies above the planes of two of the pyrazole groups in the cation, positioned 2.1-2.2 Å from each ring. The deepest Fourier hole of –1.3 $e.Å^{-3}$ 0.8 Å from Ag(34). In **2**·H_2O, the highest residual Fourier peak of +3.0 $e.Å^{-3}$ is 0.7 Å from N(44), and may represent a disorder site for this half-occupied cyano group. Attempts to model this, and other Fourier peaks in the vicinity, as disorder in the half-occupied $[Au(CN)_2]^-$ ion were unsatisfactory, however. The deepest Fourier hole of –1.9 $e.Å^{-3}$ in **2**·H_2O is close to C(33).

The unit cell of **4**·2CH_3NO_2·$(C_2H_5)_2O$ contains one formula unit, with each moiety lying on a general crystallographic position. No disorder was detected during refinement of this structure, and no restraints were applied. All non-H atoms were refined anisotropically, while H atoms were placed in calculated positions and refined using a riding model.

Other measurements.

Electrospray mass spectra were obtained using a Waters Micromass ZQ4000 spectrometer from MeCN solution. CHN microanalyses were performed by the University of Leeds Department of Chemistry microanalytical service. Infra-red spectra were obtained as nujol mulls pressed between NaCl windows between 600-4,000 cm^{-1}, using a Nicolet Avatar 360 spectrophotometer. Magnetic susceptibility measurements were obtained using a Quantum Design SQUID magnetometer in an applied field of 1000 G. Diamagnetic corrections were estimated from Pascal's constants [25], and a diamagnetic correction for the sample holder was also applied. Magnetochemical calculations and graph preparation were carried out using *SIGMAPLOT* [26].

RESULTS AND DISCUSSION

An aqueous solution of $[Fe(3\text{-bpp})_2]Cl_2$ was generated by adding 2 equiv of 3-bpp to $FeCl_2·4H_2O$ in water at room temperature. Addition of $K[Ag(CN)_2]$, $K[Au(CN)_2]$, $K[Au(NCS)_2]$ to the filtered solution immediately afforded orange precipitates, which were collected by filtration. These were sparingly soluble in common organic solvents, but they could be recrystallised on a 0.1 g scale from 2,2,2-trifluoroethanol with diethyl ether as antisolvent. Elemental microanalysis formulated these products as $[Fe(3\text{-bpp})_2][M(CN)_2]_2$ (M = Ag, **1**; M = Au, **2**) and $[Fe(3\text{-bpp})_2][Au(SCN)_2]_2·CF_3CH_2OH$ (**3**), although repeated recrystallisations were required to obtain the materials in good purity. Although **1** and **2** form

hydrate crystals under these conditions (see below), the lattice water is lost upon drying *in vacuo*. The trifluoroethanol solvent content in **3** is retained by microanalysis following prolonged drying, however. The IR spectra of the solid compounds show strong ν_{CN} absorbances at 2149 (**1**), 2147 (**2**) and 2131 cm^{-1} (**3**), which are typical values for salts of those anions [21, 27]. The ES mass spectra of **1** and **3** contain high-abundance peaks attributable to silver- and gold- 3-bpp complex ions, implying that ligand exchange between the iron and coinage metal centers takes place in solution. That explains our difficulties in preparing the compounds in pure form.

The monohydrate single crystals of **1**·H_2O and **2**·H_2O are weak diffractors at room temperature, which may reflect their mixed spin-state populations at that temperature and, for **2**·H_2O, a plate-like crystal morphology. Full structure refinements were achieved of both compounds at temperatures where they are effectively fully low-spin, 150 K for **1**·H_2O and 100 K for **2**·H_2O (see below). The two compounds are isostructural under those conditions, in the space group $P2_1/c$ (Table 1). The asymmetric units consist of one complex dication and two $[M(CN)_2]^-$ (M = Ag or Au) sites on general crystallographic positions; an additional half-anion $[M(CN)_2]^-$ site with M(34) lying on a crystallographic inversion centre; and a disordered region lying within hydrogen-bonding distance of three other groups in the lattice, that was modeled as lattice water (Fig. 1). The coinage metal atoms M(34), M(37), M(42) and their symmetry equivalents form a linear five-atom chain linked by typical argentophilic or aurophilic interactions M...M = 3.1-3.3 Å (Table 2). However the putative unit cell contents described above, $[Fe(3\text{-bpp})_2][M(CN)_2]_{2.5}\cdot H_2O$, are inconsistent with the 1:2 cation:anion ratio expected from the analytical formulations of the bulk materials. This anomaly was resolved following the observation that the atomic displacement parameters of the anion M(37)-N(46) in both structures were substantially higher than for the other two unique anion sites. Thus this anion was refined as half-occupied in the final models. In this

interpretation, the anion centred on M(42) is disordered equally between two sites sandwiched by M(34) and M(37), or M(34) and M(37^{i}) [symmetry code (i) –*x*, –*y*, –*z*] (Fig. 1).

<Insert Figure 1 and Table 2 here>

A more rigorous description of the formulation of **1**·H_2O and **2**·H_2O is therefore [Fe(3-bpp)$_2$]$_2$[M(CN)$_2$][M_3(CN)$_6$]·2H_2O (M = Ag or Au; Fig. 1), with the positions of the [M(CN)$_2$]$^-$ and [M_3(CN)$_6$]$^{3-}$ moieties being randomly distributed within each anion dyad through the crystal lattices. The bond lengths and angles at Fe(1) in both structures are as expected for low-spin iron(II) centres (Table 2), consistent with the properties of the bulk materials at the temperatures of measurement (see below), while the dimensions of the [M(CN)$_2$]$^-$ fragments are typical for those anions [11]. The cations and anions in the crystal lattices are linked by extensive hydrogen bonding (Table 3). The two N–H...N hydrogen bonds involving the fully occupied anion M(37)-N(41) (the hydrogen bonds shown in bold in Figs. 1 and 2) associate the [Fe(3-bpp)$_2$]$_2$[Ag(CN)$_2$][Ag_3(CN)$_6$]·2H_2O moieties into chains parallel to the [010] vector. The disordered anion sites M(42)-N(46) further link these chains into 2D sheets in the (001) plane, through direct N–H...N hydrogen bonding to the complex cation and *via* the lattice water (Figs. 2 and 3). Importantly the two disorder sites of M(42)-N(46) within the centrosymmetric dimer yield the same overall hydrogen-bonding connectivity pattern (Fig. 3).

<Insert Figs. 2 and 3 and Table 3 here>

There is a weak π-π interaction between pairs of [Fe(3-bpp)$_2$]$^{2+}$ cations in the lattice, involving the pyrazole substituent C(13)-C(17) and its symmetry equivalent C(13^{viii})-C(17^{viii}) [symmetry code (viii) 1–*x*, 1–*y*, –*z*]. These groups are coplanar by symmetry, and separated

by 3.55(4) (**1**) and 3.61(6) Å (**2**). Otherwise, neighbouring cations in the the lattices of **1**·H_2O and **2**·H_2O interact through van der Waals contacts only.

A similar complexation reaction using $NaBPh_4$ as the anion metathesis reagent afforded a yellow precipitate that, in contrast to **1-3**, was highly soluble in organic solvents. Recrystallisation of the powder from $MeNO_2/Et_2O$ yielded yellow plates of formula [Fe(3-bpp)$_2$][BPh_4]$_2$·2CH_3NO_2·(C_2H_5)$_2$O [**4**·2CH_3NO_2·(C_2H_5)$_2$O]. The iron centre in these crystals is almost fully high-spin at 150 K on the basis of its Fe–N bond lengths and angles (Table 2) [9], which is consistent with its yellow colouration. Only one of the four N–H groups in the cation donates a strong hydrogen bond in these crystals, to the diethyl ether solvent molecule. The other N–H donors form weak C–H...π interactions to the BPh_4^- anions (Fig. 4 and Table 3). Notably, the {[Fe(3-bpp)$_2$](C_2H_5)$_2$O}$^{2+}$ assembly is almost entirely encapsulated by BPh_4^- ions in the crystal lattice (Fig. 5), and there are no direct van der Waals contacts between complex cations in the crystal. Hence, any spin-crossover in this material would be expected to occur very gradually with temperature, as observed below. The yellow crystalline solvate decomposes and darkens in colour upon drying, yielding a dark orange powder of formula [Fe(3-bpp)$_2$][BPh_4]$_2$·$x$$H_2O$ (**4**·$x$$H_2O$; $x \approx 0.5$). The existence of a small amount of water in the bulk material, suggested by microanalysis, was confirmed by the observation of a characteristic δ{H–O–H} peak at 1647 cm^{-1} in its IR spectrum [27]. The change in colour upon drying implies that a change in spin state takes place in the complex during the desolvation process (see below).

<Insert Figures 4 and 5 here>

Solid **1-3** all undergo extremely gradual thermal spin-transitions from their variable temperature magnetic susceptibility data (Fig. 6, top). The $\chi_M T$ values for **1** (2.1 cm^3 mol^{-1} K) and **2** (1.9 cm^3 mol^{-1} K) at 300 K imply that the compounds are 55-60 % high-spin at room

temperature, since high-spin $[Fe(3\text{-bpp})_2]^{2+}$ exhibits $\chi_M T$ = 3.5±0.1 cm^3 mol^{-1} K [9, 10]. On cooling $\chi_M T$ for **1** steadily decreases to 0.3 cm^3 mol^{-1} K at 80 K, then is almost constant at that value on further cooling. Compound **2** behaves slightly differently, with $\chi_M T$ decreasing to 0.6 cm^3 mol^{-1} K at 150 K, then more slowly below that temperature to reach 0.3 cm^3 mol^{-1} K at 60 K. The low-temperature plateau $\chi_M T$ values show that spin-crossover in **1** and **2** proceeds to > 90 % completeness, with only a small residual fraction of the samples being kinetically trapped in their high-spin state at very low temperatures [28, 29]. The midpoint temperatures ($T_{½}$) of these very gradual transitions, where the high- and low-spin populations of the samples are equal, can be estimated at 251 K for **1** and 291 K for **2**. Although **3** is almost fully high-spin at room temperature ($\chi_M T$ = 3.1 cm^3 mol^{-1} K), it shows a similarly gradual thermal spin-crossover with a lower $T_{½}$ temperature of *ca.* 198 K (Fig. 6). The susceptibility of **3** plateaus at 0.6 cm^3 mol^{-1} K below 90 K, implying that this transition proceeds to *ca.* 85 % completeness. Thermal, kinetic trapping of a residual high-spin fraction of the sample often occurs in spin-transitions extending below *ca.* 100 K [30].

<Insert Figure 6 here>

Solid **4**·*x*H_2O also undergoes spin-crossover very gradually, with $T_{½}$ = 232±2 K (Fig. 6, bottom). The material is essentially low-spin below *ca.* 120 K but is still <90 % high-spin at 400 K, the highest temperature accessible to us. The different spin-states at 150 K of the bulk powder (predominantly low-spin) and the single crystalline solvate (predominantly high-spin) will be a consequence of the structural rearrangements accompanying the replacement of the organic lattice solvent by atmospheric moisture. Spin-state changes caused by solvent loss are well known in $[Fe(3\text{-bpp})_2]^{2+}$ chemistry [6, 9, 10]. The spin-state composition of **4**·*x*H_2O at room temperature (*ca.* 65 % low-spin) is also consistent with its dark orange colouration [9]. There is a clear discontinuity in the susceptibility data near room temperature, which implies there are two distinct iron populations in the sample undergoing spin-crossover over

different temperature ranges (Fig. 6). Discontinuous spin-crossover can arise from a crystallographic phase change [28, 31] or order:disorder transition [32], or from the existence of multiple lattice sites that undergo spin-crossover at different temperatures [33]. However, the discontinuity in **4**·*x*H_2O is not easily explained on the basis of the solvate crystal structure, which only has one unique iron environment in its asymmetric unit. We suggest that the discontinuity may reflect the approximate half-equivalent of lattice water in the sample, which could hydrogen bond to a fraction of the iron sites in the material. The complex molecules associated with the lattice water would undergo spin-crossover at a different, probably higher, temperature from those that are not [9, 11].

Salts of $[Ag(CN)_2]^-$, $[Au(CN)_2]^-$ or $[Au(NCS)_2]^-$ can show visible luminescence upon irradiation in the UV, in the solid state or in concentrated solutions. This arises from metal-based $d_{z^2} \rightarrow p_z$ excitations within chains of these centres linked by argentophilic or aurophilic bonding [14, 15, 21, 34]. While many such compounds are only emissive below 200 K in the solid state, significant emission at room temperature can also be sometimes observed [21, 34]. Hence the $[M_3(CN)_6]^{3-}$ centres in **1** and **2** (Fig. 1) mean that those materials, at least, had potential to show luminescent behaviour. However, no emission was observed from either compound at room temperature upon irradiation at 254 nm.

CONCLUSION

The very gradual nature of spin-crossover in **1**-**4** is unusual for salts of $[Fe(3\text{-bpp})_2]^{2+}$, which often show moderate or strong cooperativity [6, 9, 10]. This includes the previously reported cyanometallate salt $[Fe(3\text{-bpp})_2][Fe(CN)_5NO]$, whose spin-state transition occurs abruptly at 182 K with a small thermal hysteresis loop [19]. The cooperativity in $[Fe(3\text{-bpp})_2][Fe(CN)_5NO]$ is a consequence of a crystallographic phase transition during spin-

crossover, to accommodate a tilting of the nitroprusside anions in the low-spin state [19]. Since reliable structural data for **1** and **2** at higher temperatures could not be obtained, it is unclear whether a comparable phase change is involved in their spin-crossover. In any case, however, the absence of any direct hydrogen bonding or strong π-π interactions between the iron centres in **1** and **2**, and the increased rigidity of their lattices induced by Ag...Ag or Au...Au bonding, are both consistent with the observed poorly cooperative spin-crossover [35]. The gradual spin-crossover behaviour of **4** is less surprising, given the encapsulation of each cation by the anions in the lattice (Fig. 5). Gradual spin-crossover is common in BPh_4^- salts of spin-crossover cations, because the large anions act as inert spacers between the functional complex centres, thus reducing cooperativity [36].

The non-observation of room-temperature luminescence from the $[M_3(CN)_6]^{3-}$ (M = Ag or Au) centres in **1** and **2** has several potential explanations. Most likely, is simple radiative decay of the emission by coupling to lattice vibrations at such high temperatures [15]. Alternatively, the quenching of emission from the silver or gold centres may be a consequence of interactions with the iron complex cation. This could lead to energy transfer from $[M_3(CN)_6]^{3-}$ to the low-spin fraction of the iron sites in the materials, which are 40-50 % low-spin at room temperature from susceptibility measurements [12]. Finally, the strong UV $\pi \rightarrow \pi^*$ transitions from the 3-bpp ligand could preclude emission by competing with the metal-based absorptions for the incident photons.

SUPPLEMENTARY DATA

Full crystallographic data for are available on request from the Cambridge Crystallographic Data Centre, 12 Union Road, Cambridge CB2 1EZ, UK, quoting CCDC deposition number 866926–866928.

ACKNOWLEDGEMENTS

The authors thank Dr H. J. Blythe (University of Sheffield) for the susceptibility measurements, and the EPSRC for funding.

REFERENCES

[1] For recent reviews see:

a) O. Sato, J. Tao, Y.-Z. Zhang, Angew. Chem., Int. Ed. 46 (2007) 2153;

b) M. A. Halcrow, Chem. Soc. Rev. 37 (2008) 278;

c) P. Gamez, J. S. Costa, M. Quesada, G. Aromí, Dalton Trans. (2009) 7845;

d) A. Bousseksou, G. Molnár, L. Salmon, W. Nicolazzi, Chem. Soc. Rev. 40 (2011) 3313.

[2] O. Kahn, J. Krober, C. Jay, Adv. Mater. 4 (1992) 718.

[3] A. B. Gaspar, V. Ksenofontov, M. Seredyuk, P. Gütlich, Coord. Chem. Rev. 249 (2005) 2661.

[4] See *e.g.*

a) S. Dorbes, L. Valade, J. A. Real, C. Faulmann, Chem. Commun. (2005) 69;

b) K. Takahashi, H.-B. Cui, Y. Okano, H. Kobayashi, Y. Einaga, O. Sato, Inorg. Chem. 45 (2006) 5739;

c) C. Faulmann, K. Jacob, S. Dorbes, S. Lampert, I. Malfant, M.-L. Doublet, L. Valade, J. A. Real, Inorg. Chem. 46 (2007) 8548;

d) K. Takahashi, H.-B. Cui, Y. Okano, H. Kobayashi, H. Mori, H. Tajima, Y. Einaga, O. Sato, J. Am. Chem. Soc. 130 (2008) 6688;

e) A. I. S. Neves, J. C. Dias, B. J. C. Vieira, I. C. Santos, M. B. Castelo Branco, L. C. J. Pereira, J. C. Waerenborgh, M. Almeida, D. Belo, V. da Gama, CrystEngComm 11 (2009) 2160.

[5] a) M. C. Giménez-López, M. Clemente-León, E. Coronado, F. M. Romero, S. Shova, J.-P. Tuchagues, Eur. J. Inorg. Chem. (2005) 2783;

b) E. Coronado, J. R. Galán Mascarós, M. C. Giménez-López, M. Almeida, J. C. Waerenborgh, Polyhedron 26 (2007) 1838;

c) H.-Z. Kou, O. Sato, Inorg. Chem. 46 (2007) 9513;

d) M. Clemente-León, E. Coronado, M. López-Jordà, G. Mínguez Espallargas, A. Soriano-Portillo, J. C. Waerenborgh, Chem. Eur. J. 16 (2010) 2207;

e) M. Clemente-León, E. Coronado, M. López-Jordà, Dalton Trans. 39 (2010) 4903;

f) M. Clemente-León, E. Coronado, M. López-Jordà, C. Desplanches, S. Asthana, H. Wang, J.-F. Létard, Chem. Sci. 2 (2011) 1121.

[6] a) M. Clemente-León, E. Coronado, M. C. Giménez-López, F. M. Romero, Inorg. Chem. 46 (2007) 11266;

b) M. Clemente-León, E. Coronado, M. C. Giménez-López, F. M. Romero, S. Asthana, C. Desplanches, J.-F. Létard, Dalton Trans. (2009) 8087.

[7] a) G. J. Halder, C. J. Kepert, B. Moubaraki, K. S. Murray, J. D. Cashion, Science 298 (2002) 1762;

b) S. M. Neville, G. J. Halder, K. W. Chapman, M. B. Duriska, P. D. Southon, J. D. Cashion, J.-F. Létard, B. Moubaraki, K. S. Murray, C. J. Kepert, J. Am. Chem. Soc. 130 (2008) 2869;

c) S. M. Neville, G. J. Halder, K. W. Chapman, M. B. Duriska, B. Moubaraki, K. S. Murray, C. J. Kepert, J. Am. Chem. Soc. 131 (2009) 12106;

d) C. J. Adams, J. A. Real, R, E. Waddington, CrystEngComm 12 (2010) 3547.

[8] a) V. Niel, A. L. Thompson, M. C. Muñoz, A. Galet, A. E. Goeta, J. A. Real, Angew. Chem. Int. Ed. 42 (2003) 3760;

b) M. Ohba, K. Yoneda, G. Agustí, M. C. Muñoz, A. B. Gaspar, J. A. Real, M. Yamasaki, H. Ando, Y. Nakao, S. Sakaki, S. Kitagawa, Angew. Chem. Int. Ed. 48 (2009) 4767;

c) P. D. Southon, L. Liu, E. A. Fellows, D. J. Price, G. J. Halder, K. W. Chapman, B. Moubaraki, K. S. Murray, J.-F. Létard, C. J. Kepert, J. Am. Chem. Soc. 131 (2009) 10998.

[9]M. A. Halcrow, Coord. Chem. Rev. 249 (2005) 2880 and refs. therein.

[10] a) C. M. Grunert, H. A. Goodwin, C. Carbonera, J.-F. Létard, J. Kusz, P. Gütlich, J. Phys. Chem. B 111 (2007) 6738;

b) E. Coronado, J. C. Dias, M. C. Giménez-López, C. Giménez-Saiz, C. J. Gómez-García, J. Mol. Struct. 890 (2008) 215;

c) E. Coronado, M. C. Giménez-López, C. Giménez-Saiz and F. M. Romero, CrystEngComm 11 (2009) 2198;

d) I. A. Gass, S. R. Batten, C. M. Forsyth, B. Moubaraki, C. J. Schneider, K. S. Murray, Coord. Chem. Rev. 255 (2011) 2058;

e) T. D. Roberts, F. Tuna, T. L. Malkin, C. A. Kilner, M. A. Halcrow, Chem. Sci. 3 (2012) 349.

[11] S. A. Barrett, C. A. Kilner, M. A. Halcrow, Dalton Trans. 40 (2011) 12021.

[12] a) C. Piguet, C. Edder, S. Rigault, G. Bernardinelli, J.-C. G. Bünzli, G. Hopfgartner, J. Chem. Soc., Dalton Trans. (2000) 3999 and refs. therein;

b) M. Hasegawaa, F. Renz,1, T. Hara, Y. Kikuchi, Y. Fukuda, J. Okubo, T. Hoshi, W. Linert, Chem. Phys. 277 (2002) 21.

[13] a) C. A. Tovee, C. A. Kilner, J. A. Thomas, M. A. Halcrow, CrystEngComm 11 (2009) 2069;

b) T. Kosone, C. Kanadani, T. Saito, T. Kitazawa, Polyhedron 28 (2009) 1930;

c) L. Salmon, G. Molnár, D. Zitouni, C. Quintero, C. Bergaud, J.-C. Micheaud, A. Bousseksou, J. Mater. Chem. 20 (2010) 5499;

d) S. Titos-Padilla, J. M. Herrera, X.-W. Chen, J. J. Delgado, E. Colacio, Angew. Chem. Int. Ed. 50 (2011) 3290;

e) R. González-Prieto, B. Fleury, F. Schramm, G. Zoppellaro, R. Chandrasekar, O. Fuhr, S. Lebedkin, M. Kappes, M. Ruben, Dalton Trans. 40 (2011) 7564;

f) Y. Garcia, F. Robert, A. D. Naik, G. Zhou, B. Tinant, K. Robeyns, S. Michotte, L.Piraux, J. Am. Chem. Soc. 133 (2011) 15850.

[14] A. L. Balch, Struct. Bonding (Berlin) 123 (2007) 1.

[15] a) M. A. Omary, H. H. Patterson, Inorg. Chem. 37 (1998) 1060;

b) S. R. Hettiarachchi, H. H. Patterson, M. A. Omary, J. Phys. Chem. B 107 (2003) 14249.

[16] M. D. Ward, Coord. Chem. Rev. 250 (2006) 3128.

[17] a) T. Kitazawa, Y. Gomi, M. Takahashi, M. Takeda, M. Enomoto, A. Miyazaki, T. Enoki, J. Mater. Chem. 6 (1996) 119;

b) V. Niel, J. M. Martinez-Agudo, M. C. Muñoz, A. B. Gaspar, J. A. Real, Inorg. Chem. 40 (2001) 3838;

c) V. Martínez, A. B. Gaspar, M. C. Muñoz, R. Ballesteros, N. Ortega-Villar, V. M. Ugalde-Saldívar, R. Moreno-Esparza, J. A. Real, Eur. J. Inorg. Chem. (2009) 303.

[18] See *e.g.*

a) V. Niel, M. C. Muñoz, A. B. Gaspar, A. Galet, G. Levchenko, J. A. Real, Chem. Eur. J. 8 (2002) 2446;

b) A. Galet, V. Niel, M. C. Muñoz, J. A. Real, J. Am. Chem. Soc. 125 (2003) 14224;

c) V. Niel, A. L. Thompson, A. E. Goeta, C. Enachescu, A. Hauser, A. Galet, M. C. Muñoz, J. A. Real, Chem. Eur. J. 11 (2005) 2047;

d) G. Agustí, M. C. Muñoz, A. B. Gaspar, J. A. Real, Inorg. Chem. 47 (2008) 2552;

e) T. Kosone, Y. Suzuki, S. Ono, C. Kanadani, T. Saito, T. Kitazawa, Dalton Trans. 39 (2010) 1786.

[19] K. H. Sugiyarto, W.-A. McHale, D. C. Craig, A. D. Rae, M. L. Scudder, H. A. Goodwin, Dalton Trans. (2003) 2443.

[20] Y. Lin, S. A. Lang jr., J. Heterocycl. Chem. 14 (1977) 345.

[21] a) N. L. Coker, J. A. K. Bauer, R. C. Elder, J. Am. Chem. Soc. 126 (2004) 12;

b) R. K. Arvapally, P. Sinha, S. R. Hettiarachchi, N. L. Coker, C. E. Bedel, H. H. Patterson, R. C. Elder, A. K. Wilson, M. A. Omary, J. Phys. Chem. C 111 (2007) 10689.

[22] G. M. Sheldrick, Acta Crystallogr., Sect. A 64 (2008) 112.

[23] L. J. Barbour, J. Supramol. Chem., 2001, 1, 189.

[24] POVRAY v. 3.5, Persistence of Vision Raytracer Pty. Ltd., Williamstown, Victoria, Australia, 2002. http://www.povray.org.

[25] C. J. O'Connor, Prog. Inorg. Chem. 29 (1982) 203.

[26] SIGMAPLOT, v. 8.02, SPSS Scientific Inc., Chicago IL, 2002.

[27] K. Nakamoto, Infrared and Raman Spectra of Inorganic and Coordination Compounds, Part B, 5th edn., Wiley Interscience, New York, 1997, p. 54 and 105-113.

[28] V. A. Money, C. Carbonera, J. Elhaïk, M. A. Halcrow, J. A. K. Howard and J.-F. Létard, Chem. Eur. J. 13 (2007) 5503.

[29] a) G. Ritter, E. König, W. Irler, H. A. Goodwin, Inorg. Chem. 17 (1978) 224;

b) T. Buchen, H. Toftlund, P. Gütlich, Chem. Eur. J. 2 (1996) 1129;

c) R. Hinek, H. Spiering, P. Gütlich, A. Hauser, Chem. Eur. J. 2 (1996) 1435;

d) N. Moliner, A. B. Gaspar, M. C. Muñoz, V. Niel, J. Cano, J. A. Real, Inorg. Chem. 40 (2001) 3986;

e) A. B. Gaspar, M. C. Muñoz, N. Moliner,V. Ksenofontov, G. Levchenko, P. Gütlich, J. A. Real, Monatsh. Chem. 134 (2003) 285.

[30] See *e.g.*

a) N. Moliner, A. B. Gaspar, M. C. Muñoz, V. Niel, J. Cano, J. A. Real, Inorg. Chem. 40 (2001) 3986;

b) O. Roubeau, A. F. Stassen, I. F. Gramage, E. Codjovi, J. Linarés, F. Varret, J. G. Haasnoot, J. Reedijk, Polyhedron 20 (2001) 1709;

c) V. A. Money, C. Carbonera, J. Elhaïk, M. A. Halcrow, J. A. K. Howard, J.-F. Létard, Chem. Eur. J. 13 (2007) 5503.

[31] a) D. Chernyshov, M. Hostettler, K. W. Törnroos, H.-B. Bürgi, Angew. Chem. Int. Ed. 42 (2003) 3825;

b) W. Hibbs, P. J. van Koningsbruggen, A. M. Arif, W. W. Shum, J. S. Miller, Inorg. Chem. 42 (2003) 5645;

c) S. Bonnet, M. A. Siegler, J. S. Costa, G. Molnár, A. Bousseksou, A. L. Spek, P. Gamez, J. Reedijk, Chem. Commun. (2008) 5619;

d) T. Sato, K. Nishi, S. Iijima, M. Kojima, N. Matsumoto, Inorg. Chem. 48 (2009) 7211;

e) V. Martínez, A. B. Gaspar, M. C. Muñoz, G. V. Bukin, G. Levchenko, J. A. Real, Chem. Eur. J. 15 (2009) 10960.

[32] a) V. A. Money, J. Elhaïk, I. R. Evans, M. **A**. Halcrow, J. A. K. Howard, Dalton Trans. (2004) 65;

b) K. W. Törnroos, M. Hostettler, D. Chernyshov, B. Vangdal, H.-B. Bürgi, Chem. Eur. J. 12 (2006) 6207;

c) G. S. Matouzenko, D. Luneau, G. Molnár, N. Ould-Moussa, S. Zein, S. A. Borshch, A. Bousseksou, F. Averseng, Eur. J. Inorg. Chem. (2006) 2671;

d) B. A. Leita, S. M. Neville, G. J. Halder, B. Moubaraki, C. J. Kepert, J.-F. Létard, K. S. Murray, Inorg. Chem. 46 (2007) 8784;

e) G. A. Craig, J. S. Costa, O. Roubeau, S. J. Teat, G. Aromí, Chem. Eur. J. 17 (2011) 3120.

[33] a) D. Boinnard, A. Bousseksou, A. Dworkin, J.-M. Savariault, F. Varret, J.-P. Tuchagues, Inorg. Chem. 33 (1994) 271;

b) G. S. Matouzenko, J.-F. Létard, S. Lecoeq, A. Bousseksou, L. Capes, L. Salmon, M. Perrin, O. Kahn, A. Collet, Eur. J. Inorg. Chem. (2001) 2935;

c) A. J. Simaan, M.-L. Boillot, R. Carrasco, J. Cano, J.-J. Girerd, T. A. Mattioli, J. Ensling, H. Spiering, P. Gütlich, Chem. Eur. J. 11 (2005) 1779;

d) M. S. Shongwe, B. A. Al-Rashdi, H. Adams, M. J. Morris, M. Mikuriya, G. R. Hearne, Inorg. Chem. 46 (2007) 9558;

e) C.-F.Sheu, S. Pillet, Y.-C. Lin, S.-M. Chen, I.-J. Hsu, C. Lecomte, Y. Wang, Inorg. Chem. 47 (2008) 10866;

f) J. Klingele, D. Kaase, M. H. Klingele, J. Lach, S. Demeshko, Dalton Trans. 39 (2010) 1689.

[34] a) N. Nagasundaram, G. Roper, J. Biscoe, J. W. Chai, H. H. Patterson, N. Blom, A. Ludi, Inorg. Chem. 25 (1986) 2947;

b) M. J. Katz, T. Ramnial, H.-Z. Yu, D. B. Leznoff, J. Am. Chem. Soc. 130 (2008) 10662.

[35] M. A. Halcrow, Chem. Soc. Rev. 40 (2011) 4119.

[36] See *e.g.*

a) K. H. Sugiyarto, H. A. Goodwin, Aust. J. Chem. 40 (1987) 775;

b) D. Onggo, H. A. Goodwin, Aust. J. Chem. 44 (1991) 1539;

c) R. Boča, P. Baran, M. Boča, L. Dlháň, H. Fuess, W. Haase, W. Linert, B. Papánková, R. Werner, Inorg. Chim. Acta 278 (1998) 190;

d) Z. Ni, M. P. Shores, J. Am. Chem. Soc. 131 (2009) 32;

e) T. M. Ross, S. M. Neville, D. S. Innes, D. R. Turner, B. Moubaraki, K. S. Murray, Dalton Trans. 39 (2010) 149.

Table 1. Experimental details for the single crystal structure determinations in this work.

	1	**2**	**4**·2CH_3NO_2·$(C_2H_5)_2O$
Formula	$C_{26}H_{18}Ag_2FeN_{14}·H_2O$	$C_{26}H_{18}Au_2FeN_{14}·H_2O$	$C_{76}H_{74}B_2FeN_{12}O_5$
M_r	816.15	994.34	1312.94
Crystal size (mm^3)	0.43 x 0.31 x 0.15	0.34 x 0.33 x 0.03	0.37 x 0.32 x 0.15
Crystal system	monoclinic	monoclinic	monoclinic
Space group	$P2_1/c$	$P2_1/c$	$P2_1/n$
a (Å)	17.1963(9)	17.487(4)	11.4029(9)
b (Å)	14.4039(7)	14.433(3)	34.872(3)
c (Å)	13.9172(8)	14.116(3)	17.3213(15)
β (°)	100.241(2)	99.87(3)	93.945(4)
V ($Å^3$)	3392.3(3)	3510.0(12)	6871.4(10)
Z	4	4	4
T (K)	150(2)	100(2)	150(2)
ρ_{calc} ($g.cm^{-3}$)	1.598	1.882	1.269
μ (mm^{-1})	1.607	8.787	0.281
Measured reflections	31518	35635	130085
Independent reflections	8391	8440	18263
R_{int}	0.029	0.049	0.031
Observed reflections [$I > 2\sigma(I)$]	6267	6379	14611
Data, restraints, parameters	8391, 0, 424	8440, 0, 404	18263, 0, 869
$R_1(I > 2\sigma(I))$[a], wR_2(all data)[b]	0.073, 0.221	0.064, 0.177	0.043, 0.126
GOF	1.134	1.160	1.031
$\Delta\rho_{min}$, $\Delta\rho_{max}$ ($e.Å^{-3}$)	–1.30, 1.51	–1.86, 3.04	–0.52, 0.84

[a] $R = \Sigma\,[\,|F_o| - |F_c|\,] / \Sigma|F_o|$ [b] $wR = [\Sigma w(F_o^2 - F_c^2) / \Sigma wF_o^4]^{1/2}$

Table 2. Selected bond lengths (Å) and angles (°) in the single crystal *X*-ray structures in this work. The atom numbering scheme shown in Figure 1 is used for all three structures.

Symmetry code (i): *–x*, *–y*, *–z*.

	1·H_2O (M = Ag)	**2**·H_2O (M = Au)	**4**·$2CH_3NO_2$·$(C_2H_5)_2O$
Fe(1)–N(2)	1.934(5)	1.962(8)	2.0944(12)
Fe(1)–N(9)	1.969(5)	1.987(9)	2.1627(13)
Fe(1)–N(14)	1.972(5)	1.994(9)	2.1635(14)
Fe(1)–N(18)	1.940(5)	1.970(8)	2.0927(12)
Fe(1)–N(25)	1.969(6)	1.997(10)	2.1932(13)
Fe(1)–N(30)	1.967(5)	2.001(8)	2.1944(15)
M(34)–C(35)	2.025(10)	2.006(12)	–
M(37)–C(38)	2.054(7)	2.001(10)	–
M(37)–C(40)	2.057(7)	2.019(10)	–
M(42)–C(43)	2.041(15)	1.996(18)	–
M(42)–C(45)	2.050(13)	1.993(16)	–
M(34)…M(42)	3.2482(12)	3.3067(11)	–
M(37)…M(42)	3.1299(13)	3.2244(11)	–
N(2)–Fe(1)–N(9)	78.9(2)	78.8(4)	75.45(5)
N(2)–Fe(1)–N(14)	78.8(2)	78.7(3)	75.49(5)
N(2)–Fe(1)–N(18)	179.1(2)	179.0(3)	176.24(5)
N(2)–Fe(1)–N(25)	100.4(2)	101.1(4)	102.02(5)
N(2)–Fe(1)–N(30)	102.1(2)	101.9(3)	107.17(5)
N(9)–Fe(1)–N(14)	157.7(2)	157.5(4)	150.82(5)
N(9)–Fe(1)–N(18)	101.5(2)	102.2(4)	101.72(5)
N(9)–Fe(1)–N(25)	92.7(2)	92.8(4)	90.49(5)
N(9)–Fe(1)–N(30)	90.5(2)	91.8(4)	93.36(5)
N(14)–Fe(1)–N(18)	100.7(2)	100.3(3)	107.19(5)
N(14)–Fe(1)–N(25)	92.0(2)	92.7(4)	93.01(5)
N(14)–Fe(1)–N(30)	93.4(2)	91.5(4)	97.58(5)
N(18)–Fe(1)–N(25)	78.9(2)	78.8(4)	75.37(5)
N(18)–Fe(1)–N(30)	78.7(2)	78.3(3)	75.29(5)
N(25)–Fe(1)–N(30)	157.6(2)	157.1(3)	150.59(5)
C(35) –M(34) –C(35^{i})	180	180	–
C(38) –M(37) –C(40)	173.6(3)	174.8(5)	–
C(43) –M(42) –C(45)	173.0(6)	178.3(7)	–

Table 3. Hydrogen bonding parameters in the single crystal *X*-ray structures in this work (Å, °). The symmetry codes are the same as in Fig. 1: (i) –*x*, –*y*, –*z*; (ii) *x*, ½–*y*, ½+*z*; (iii) *x*, ½–*y*, –½+*z*; (iv) *x*, 1+*y*, *z*; (vii) –*x*, ½+*y*, ½–*z*.

	D–H	H…A	D…A	D–H…A
1·H_2O				
N(10)–H(10)...N(44^{ii})	0.88	1.87	2.749(11)	174.4
N(15)–H(15)...N(41)	0.88	1.93	2.782(8)	164.0
N(26)–H(26)...N(46^{iii})	0.88	1.86	2.734(12)	172.9
N(31)–H(31)...N(39^{iv})	0.88	1.89	2.770(8)	175.4
O(47A)/O(47B)...N(36)	–	–	2.95/2.94	–
O(47A)... N(44^{ii})	–	–	2.55	–
O(47B)...N(46^{vii})	–	–	2.84	–
2·H_2O				
N(10)–H(10)...N(44^{ii})	0.88	1.95	2.81(2)	163.9
N(15)–H(15)...N(41)	0.88	1.96	2.810(13)	163.0
N(26)–H(26)...N(46^{iii})	0.88	1.92	2.794(19)	169.2
N(31)–H(31)...N(39^{iv})	0.88	1.92	2.800(13)	178.5
O(47A)/O(47B)...N(36)	–	–	3.02/2.98	–
O(47A)... N(44^{ii})	–	–	2.76	–
O(47B)...N(46^{vii})	–	–	2.77	–
4·2CH_3NO_2·$(C_2H_5)_2O$				
N(10)–H(10)...O(86)	0.88	1.95	2.8224(18)	174.1
N(15)–H(15)…[C(53)-C(58)][a]	0.88	2.59	3.257	133.3
N(26)–H(26)…[C(60)-C(65)][a]	0.88	2.44	3.236	149.8
N(26)–H(26)…[C(41^{ii})-C(46^{ii})][a]	0.88	2.72	3.340	128.7

[a]Metric parameters are calculated from the centroids of the phenyl ring acceptor groups.

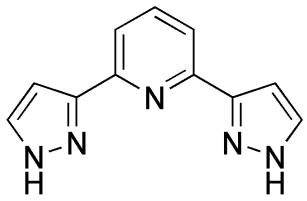

3-bpp

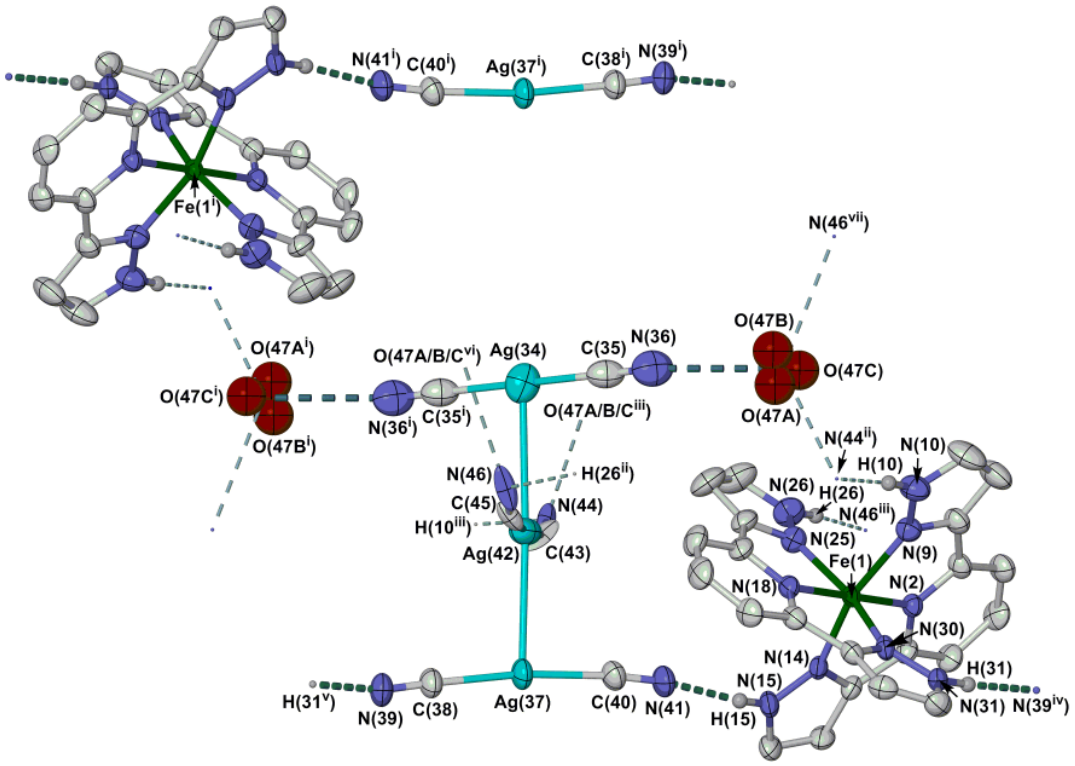

Figure 1. View of the centrosymmetric $[Fe(3\text{-bpp})_2]_2[Ag(CN)_2][Ag_3(CN)_6]\cdot 2H_2O$ moiety in the crystal structure of **1**·H_2O. All C-bound H atoms are omitted for clarity and displacement ellipsoids are at the 50% probability level, except for H atoms which have arbitrary radii. Only one of the two sites for the disordered $[Ag(CN)_2]^-$ fragment Ag(42)-N(46) is shown, and the half-occupied hydrogen bonds involving this disordered residue are de-emphasised. Symmetry codes: (i) –*x*, –*y*, –*z*; (ii) *x*, ½–*y*, ½+*z*; (iii) *x*, ½–*y*, –½+*z*; (iv) *x*, 1+*y*, *z*; (v) *x*, –1+*y*, *z*; (vi) –*x*, –½+*y*, ½–*z*; (vii) –*x*, ½+*y*, ½–*z*.

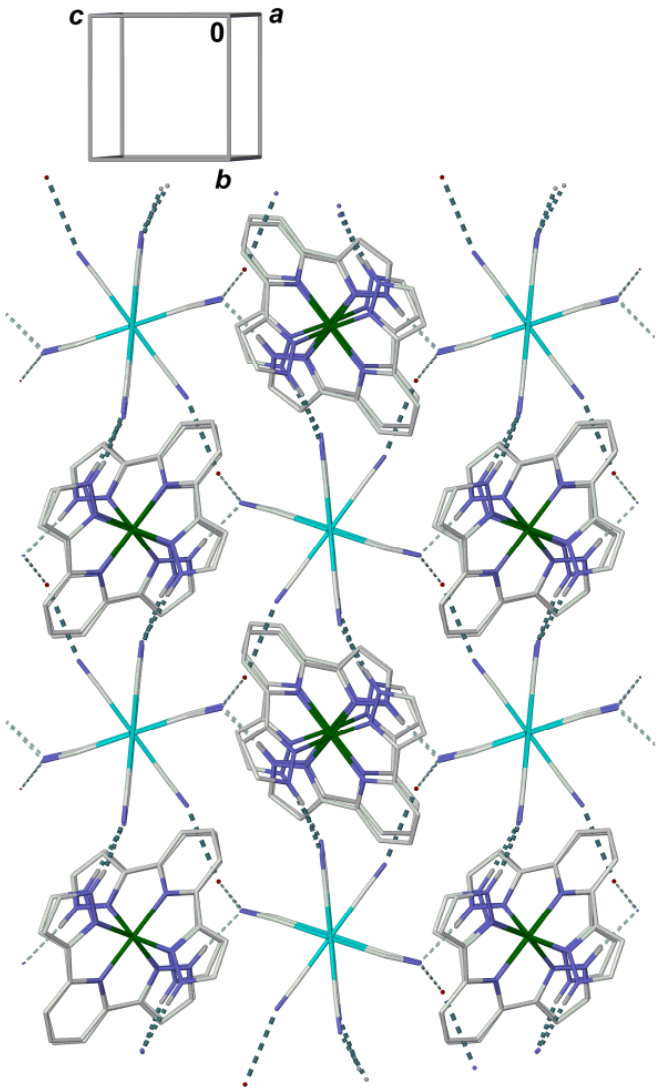

Figure 2. Partial packing diagram of **1**·H_2O, showing the association of the [Fe(3-bpp)$_2$]$_2$[Ag(CN)$_2$][Ag$_3$(CN)$_6$]·2H_2O units into 2D hydrogen-bonded arrays. All C-bound H atoms are omitted for clarity and all atoms which have arbitrary radii. The half-occupied hydrogen bonds involving the disordered $[Ag(CN)_2]^-$ fragment Ag(42)-N(46) residue are de-emphasised. The orientation of the unit cell in this arbitrary view is also shown.

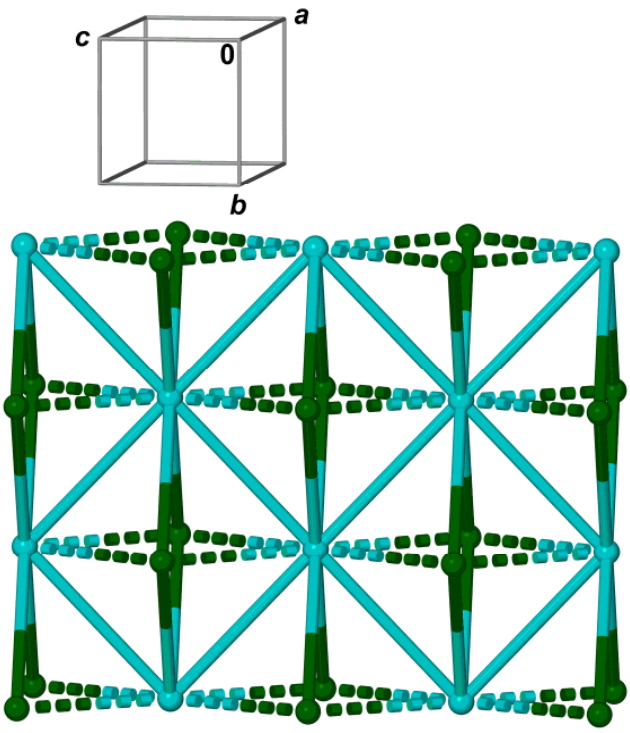

Figure 3. The 2D hydrogen-bonded network topology in **1**·H_2O, involving the $[Fe(3\text{-bpp})_2]^{2+}$ (cyan) and $\{[Ag(CN)_2][Ag_3(CN)_6]\}^{4-}$ moieties (green) as connectors. The dashed connections between cation and anion connectors proceed through the disordered $[Ag(CN)_2]^-$ fragment Ag(42)-N(46), and only one out of any pair of these connections is occupied in a random manner.

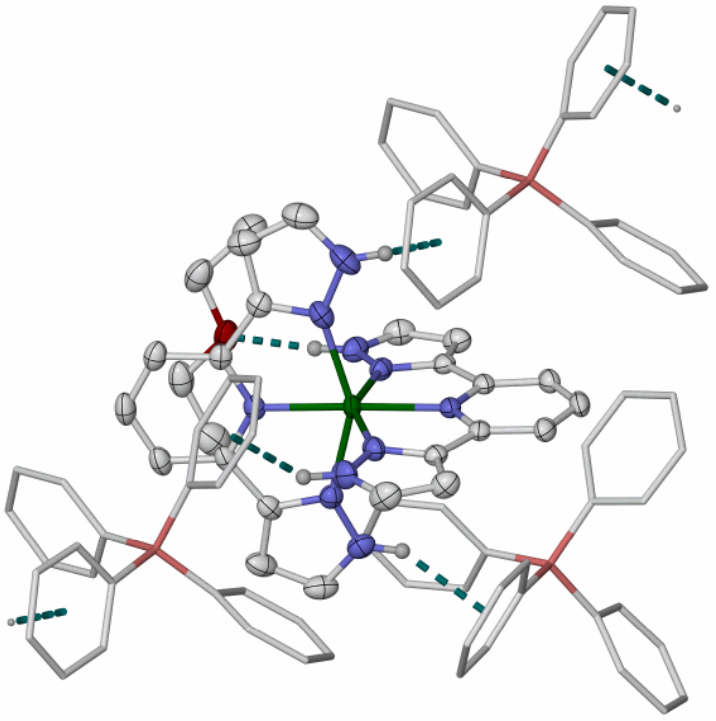

Figure 4. View of the hydrogen bonding interactions in **4**·2CH_3NO_2·$(C_2H_5)_2O$. Thermal ellipsoids are at the 50% probability level except for the BPh_4^- ions, which have arbitrary radii, while C-bound H atoms have been omitted for clarity. Colour code: C, white; H, grey; B, pink; Fe, green; N, blue; O, red.

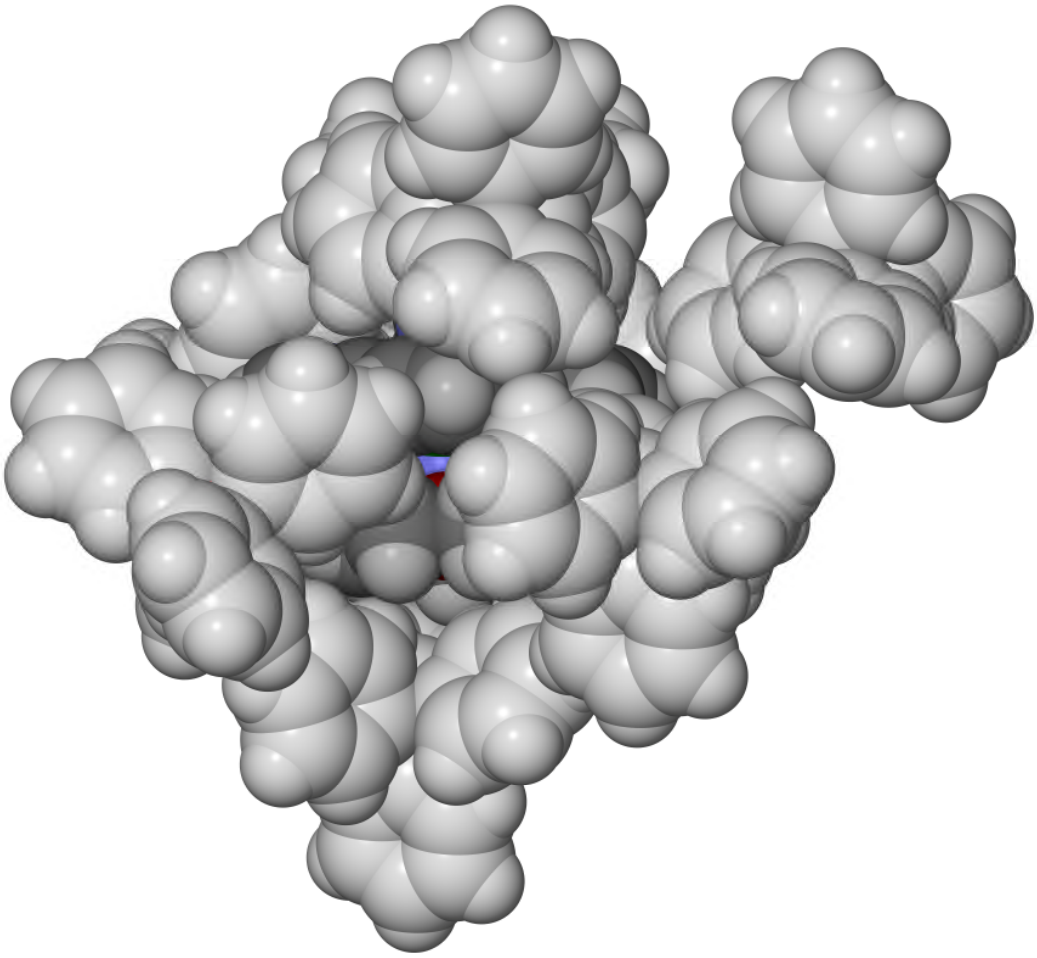

Figure 5 Partial space-filling packing diagram of **4**·2CH_3NO_2·$(C_2H_5)_2O$, showing the almost complete encapsulation of the {[Fe(3-bpp)$_2$]·$(C_2H_5)_2O$}$^{2+}$ moiety by BPh_4^- anions. The nitromethane solvent molecules have been omitted, but are not part of the encapsulated species. Colour code: BPh_4^- anion, white; C{cation, diethyl ether}, dark grey; H{cation, diethyl ether}, light grey; Fe, green; N, blue; O, red.

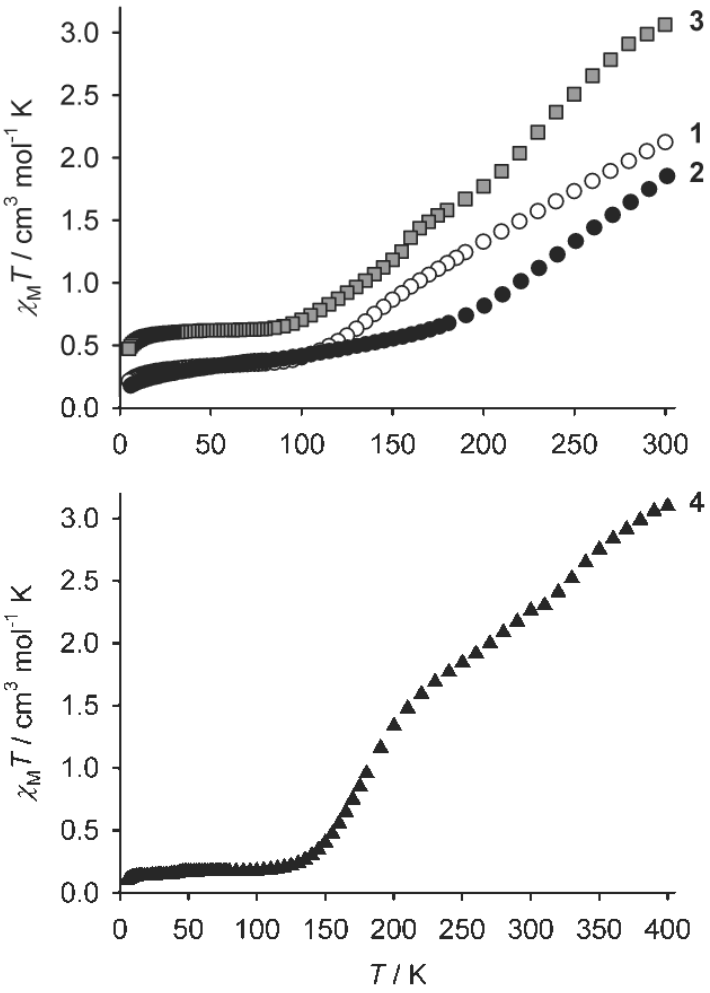

Figure 6. Variable temperature magnetic susceptibility data for the compounds in this work.